ACS APPLIED BIO MATERIALS

www.acsabm.org Article

Three-Dimensional Circular Surface Curvature of a Spherule-Based Electrode for Selective Signaling and Dynamic Mobility of Norepinephrine in Living Cells

Mohammed Y. Emran, Mohamed A. Shenashen, Sherif A. El-Safty,* Mahmoud M. Selim, Takashi Minowa, and Ahmed Elmarakbi

Cite This: https://dx.doi.org/10.1021/acsabm.0c00882 Read Online

ACCESS | Metrics & More | Article Recommendations | Supporting Information

ABSTRACT: A highly sensitive protocol for signaling norepinephrine (NEP) in human fluids and neuronal cell line models should be established for clinical investigation of some neuronal diseases. A metal-free electrode catalyst was designed based on a sulfur-doped carbon spheroidal surface (S-CSN) and employed as a transducing element for selective signaling of NEP in biological samples. The designed electrode of S-CSN features a spherical construct and curvature surface to form a spheroidal nanolayer with an average layer size of <2 nm. S-CSN shows surface topography of a circular surface curvature with a rugged surface texture, ridge ends, and free open spaces between interlayers. The rich-space diversity surfaces offer highly active surface with facile molecular/electron diffusion, multi-diffusive centers, and high target loading along with in-/out-of-plane circular spheres of the S-CSN surface. The active doping of S atoms onto the carbon-based electrode creates an active transducing element with many active sites, strong binding to targeted molecules, facile diffusion of charges/molecules, long-term durability, and dense reactive exposure sites for signaling NEP at ultratrace levels. S-CSN could be a sensitive and selective nanosensor for signaling NEP and establishing a sensing protocol with high stability and reproducibility. The sensory protocol based on S-CSN exhibits high sensitivity and selectivity with a low detection limit of 0.001 μM and a wide linear range of 0.01−0.8 μM. The in vitro sensory protocol for NEP secreted from living cells (neuronal cell line model) under stimulated agents possesses high sensitivity, low cytotoxicity, and high biocompatibility. These results confirm the successful establishment of NEP sensor in human blood samples and neuronal cells for clinical investigation.

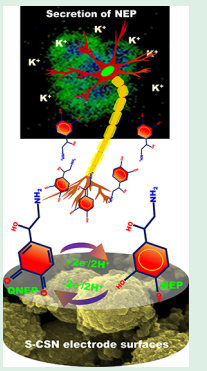

KEYWORDS: *norepinephrine, biosensor, sulfur-doped carbon-based materials, nanoporous carbon, cytotoxicity and biocompatibility, living cells*

1. INTRODUCTION

Norepinephrine (NEP), epinephrine (EPI), and dopamine (DA) are biogenic amines and regarded as monoamine neurotransmitters. Neurotransmitters play a significant role in various biological activities and function as signal transport elements in the brain and central nervous system.[1−4] The secretion of NEP from the adrenal gland usually increases under high-stress conditions, fighting, and any dangerous situation. This secretion increases the blood flow for muscles and brain as oxygen and glucose production support.[5−8] Moreover, NEP is used in the treatment of diseases such as hypertension, heart disease, diabetes, and anxiety.[1,5,7] The fluctuation of NEP levels acts as a biomarker for neurological diseases, such as schizophrenia, Parkinson's disease, and Alzheimer's disease.[9−11] In this regard, scholars have focused on establishing a highly sensitive protocol with long-term stability, on-site measurement, and high economic value for detection of NEP in human blood samples, brain slices, and living cells for clinical and neurological applications.

Controlled detection of NEP can be conducted using various analytical techniques, such as high-performance liquid chromatography,[12] fluorescence microscopy,[13,14] and electrochemistry.[3,15,16] Most of these techniques are sensitive and selective but require sophisticated procedures, time-consuming processes due to sampling preparation, highly expensive machines, and highly trained technician. Electrochemical techniques exhibit high sensitivity and selectivity, ease of use, and fast response and are suitable for in vivo and in vitro applications.[16−18] Thus, electrochemical NEP sensors/biosensors are widely used given their high selectivity in the presence of other interfering molecules.[3,15,16,19] Several approaches based on the design of modified electrodes have been established for detection of NEP; these electrodes include functionalized MWCNTs with electrodeposited luteolin, poly(trypan blue)-modified GCE, 5-amino-3′,4′-dimethyl-

Received: July 16, 2020
Accepted: October 15, 2020

biphenyl-2-ol (5ADB), and ZnO/CNTs.[15,19−21] The ITO-electrode modified with CN@NiO with novel broccoli-shaped NiO was used for selective signaling of NEP in living cells. The designed electrode showed high sensitivity, good selectivity in the presence of potentially interfering species, high stability, and reproducibility.[3]

The simple and controlled synthesis and construction of carbon-based materials as sensors and biosensor-based electrodes have attained great interest.[4,8,22−24] Various types of carbon-based materials have been used as working materials due to their good electrochemical properties, easy fabrication, and facile functionality; such materials include graphene, carbon nanotubes, fullerenes, diamond, carbon nanomaterials, and their composites.[4,8,24−28] Significant properties such as large surface area, good mechanical stability, good conductivity, easy fabrication and functionalization, and composite formation within the metal and/or metal oxides have gained particular interest in various fields, such as biosensing, water treatment, and energy.[28−36] Several approaches have been reported for enhancing the activity of carbon-based materials by doping the carbon chain with nonmetal heteroatoms, such as boron (B), phosphorus (P), nitrogen (N), and sulfur (S).[4,8,22,37−40] Doping of S atoms in the carbon chain enhances the electrochemical activity. The mechanism of action remains unclear because the electronegativity of S (2.58) is close to C (2.55). Thus, the action of S atoms on the activity of carbon materials may be related to increased electron spin density and outer surface functionalization by sulfur groups.[41,42] The active interfacial surface based on the S-doped carbon offers a highly electrochemical surface with functionalized active sites, high molecular loading, and fast charge transport.[41,42] Therefore, the function of chemical components of S-doped carbon-based materials and surface topography of curvature, meso-grooves, vortices, ridge ends, rugged surfaces, and nanoplates play key roles in establishing a highly sensitive sensory protocol for NEP detection.

Herein, spheroidal S-doped carbon-based materials were synthesized and employed for sensitive and selective signaling of NEP in human blood serum and a neuronal cell line model. S-CSN acts as a signaling transduction element of the electro-oxidation process on the electrode surface and exhibits fast response, low charge resistance, and numerous active centers. S-CSN has a spheroidal morphology with stacked nanolayers, rough surface texture, bundle surface meshes, ridge ends with a 3D orientation, S-doped graphitic carbon, and a microporous network. Furthermore, the surface topography of meso-grooves, voids, protuberances, and interfaces running over the outer surface of electrodes is woven into tightly folded sensor surfaces. Therefore, S-CSN ascertains a highly active interfacial surface for facile diffusion of targeted molecules. NEP strongly binds to the S-CNS surface and is oxidized with active signaling transduction through a sensitive, selective, facile, stable, and reproducible protocol. Real-time monitoring of NEP in various environments, such as human blood serum and living cells (acting as a neuronal cell model), was conducted using the S-CNS-modified electrode (Scheme 1). The designed S-CNS-based nanosensor showed high sensitivity, good selectivity, high stability, good reproducibility, low cytotoxicity, and high biocompatibility for in vitro detection of NEP.

Scheme 1. Design of the Sensing Assay Based on S-CNS For Detection of NEP Secreted from Living Cells[a]

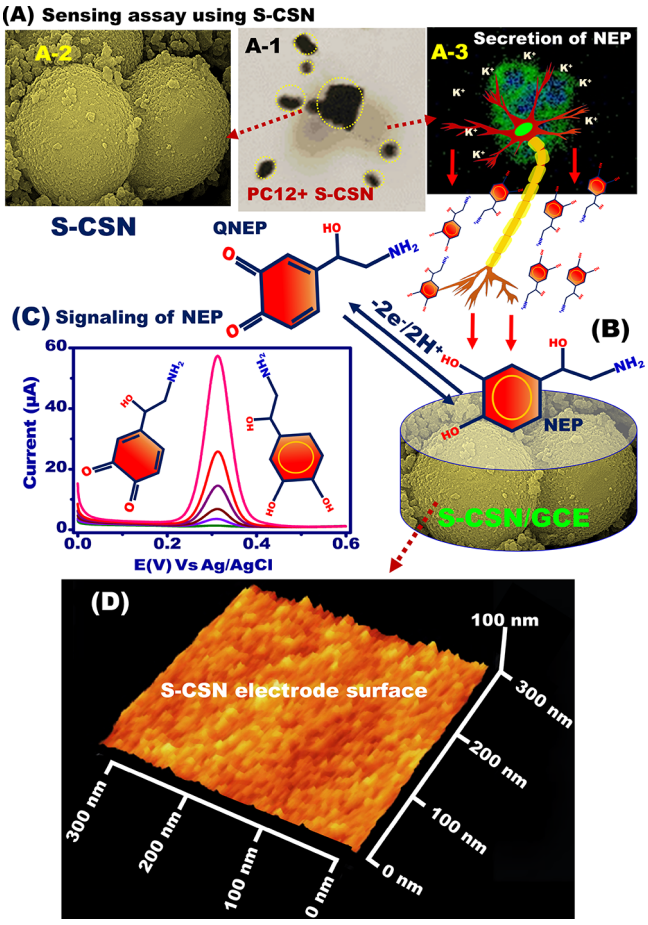

[a](A-2) S-CSN geometric structure of 3D circular surface curvature of spherules. (A-1) Incubation of S-CSN with the neuronal cell line model (PC12). (A-3) PC12 synthesis of NEP with the amount of liberated NEP increasing as the KCl concentration (stimulated agent) increases. (B, C) NEP sensor based on S-CNS/GCE transduces the electro-oxidation signal of NEP using SWV measurements. (D) Atomic force microscopy (AFM) image of S-CSN.

2. EXPERIMENTAL SECTION

2.1. Electrode Synthesis and Fabrication of 3D Circular S-Doped Carbon Spheroidal Surfaces of S-CSN. *2.1.1. Synthesis of 3D Circular S-Doped Carbon Spheroidal Surfaces.* Controlled formation of S-doped carbon-dense spherical aligned nanolayers (S-CSN) was conducted based on a simple hydrothermal treatment (HT) of hydrocarbons such as glucose and thiourea in the presence of capping agent F127.[8,24] The synthesis procedure and condition were controlled as follows. Thiourea, α-D-glucose, Pluronic F127, and distilled H_2O were mixed with the following ratios 0.25:1:1:32.5 and 0.5:1:1:32.5. The solutions were sonicated for 1 h and stirred for 2 h. Samples 1 and 2 were transferred into 100 mL Teflon-lined autoclaves and supported at 180 °C for 24 h. After cooling, a black precipitate of S-CSNs was formed. The S-CSN materials were washed many times with water/ethanol and dried at 60 °C for 24 h. For complete carbonization, the S-CSN materials were calcined at 800 °C under N_2 flow for 4 h with a step temperature increase of 5 °C/min and named S-CSN-1 and S-CSN-2.

2.2. Fabrication of 3D Circular S-Doped Carbon Spheroidal Surfaces (S-CSN) as Working Materials. The electrode fabrication for sensing of NEP was done as follows: (a) Material ink formation was performed by diffusing 5 mg of S-CSN-1 and S-CSN-2 in 1 mL of distilled H_2O, and they were further used for electrode modifications.

https://dx.doi.org/10.1021/acsabm.0c00882
ACS Appl. Bio Mater. XXXX, XXX, XXX−XXX

Scheme 2. Schematic Formation of S-CSN with Starting Materials Glucose as the Carbon Source, Thiourea as the S Atom Source, and F127 as a Directing Agent[a]

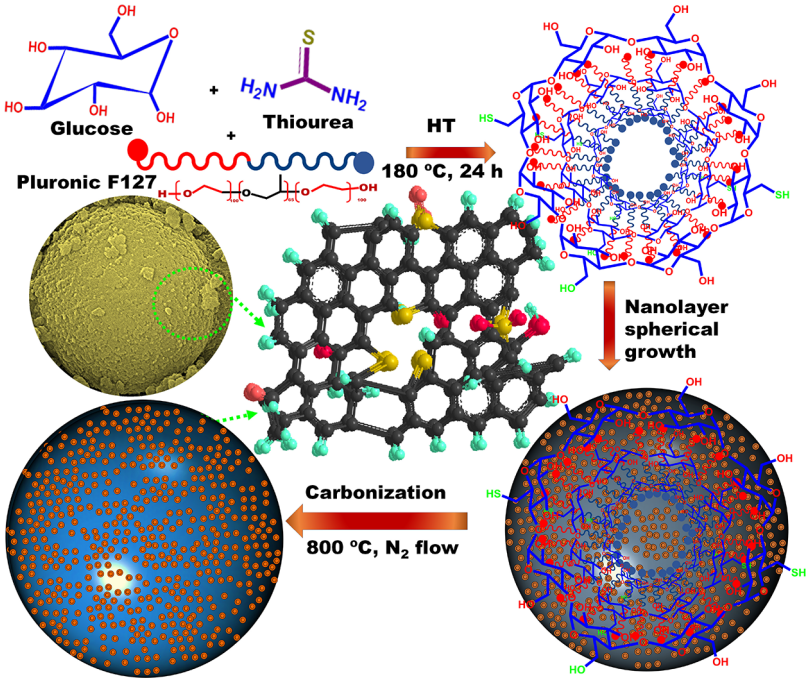

[a]With varying the thiourea concentration, two materials were synthesized and named S-CSN-1 and S-CSN-2.

(b) The glassy carbon electrode (GCE) (diameter 3.0 mm) was cleaned by polishing the electrode surface to be like a mirror using 0.05 μM alumina slurry and then polishing with a diamond slurry. At every step, the electrodes were washed with distilled H_2O every sweep. After that, the electrode was sonicated in an acetone and distilled H_2O solution for 30 min. (c) The multidimensional surface electrode of S-CSN was designed by formation of a thin layer at the GCE surface based on drop-casting of 20 μL of S-CSN-1 and S-CSN-2 and then keeping it dry at room temperature. (d) The working electrodes were activated using continuous cyclic voltammetry sweeps for 10 cycles within a potential window of 0.0−1.8 V in 0.1 M PBS (pH = 7) at a scan rate of 100 mV s^{-1}.

2.3. Cytotoxicity. The cytotoxicity of S-CSN-1 on the PC12 cells was investigated using a Cell Counting Kit-8 (CCK-8) assay. The PC12 cells (5×10^5 cells/mL) were moved onto 96-well microplates and kept in an incubator at 37 °C under 5% CO_2/95% air for 24 h. Then, various amounts of S-CSN-1 were added (10 mL of 10, 20, 50, 100, and 200 μg/mL) and incubated for 48 h. The CCK-8 solution (10 μL, 5 mg/mL) was added to each well and then incubated for 2−4 h. After that, the incubated cells were measured using a microplate reader at an absorbance of 450 nm.

2.4. Cell Culture and In Vitro Study. For cell culture growth and passaging of PC12 cells, the PC12 cells were passaged every 6 days and kept in an incubator under 5% CO_2 at 37 °C. The medium was changed two times a week throughout the lifetime of all cultures. The medium was prepared as follows: 50 mL of fetal bovine serum (FBS) and 50 mL of heat-inactivated serum were added to 500 mL of Dulbecco's modified Eagle's medium (DMEM).

For PC12 cell visualization experiments using S-CSN-1, 5×10^5 PC12 cells/mL was sowed in a 6-well plate for 24 h and kept in an incubator. The cells were stained with phalloidin 488 (1/500 mL) in PBS for F-actin staining and were stained with 4′,6-diamidino-2-phenylindole (DAPI) (1/1000 mL) in PBS for nuclear counterstaining for 5 min. Finally, the PC12 cells' images were captured at ambient temperature by confocal laser scanning microscopy (Leica TCS SPE5 X). PC12 cells were incubated with 20 μL of various amounts of KCl (0−50 mM) to study the effect of K^+ ions on the amount of NEP secreted. The solution was incubated in a humid chamber under 5% CO_2 at 37 °C for 30 min and centrifuged. The supernatant was used to evaluate the liberation of NEP from PC12 cells.

3. RESULTS AND DISCUSSION

3.1. 3D Circular Curvature Surface Design of S-Doped CSN for Selective Monitoring of NEP. Scheme 1 shows the effective synthesis of the 3D circular surface electrode based on S-CSN. The construction of the 3D circular surface of the S-doped carbon-based electrode ascertains the modulation of highly active interfacial surfaces. The active surface modulation of multiple architectures, geometries, and a mixture of various heterogeneous constructs led to the formation of high loading and wide interactive surfaces. The variable geometries of the 3D circular surface of the S-CSN-based electrode conjugated with meso-grooves, jugged texture, and ridge ends were designed. S-CSN generated a highly sensitive and selective nanosensor for screening of NEP with powerful molecular diffusion through outward/inward and then upward/downward entrances and multiple discharge rates. Therefore, the geometry and chemical composition of S-CSN could be utilized to design a selective sensor for real-time sensing of NEP secreted from the neuronal cell line model.

3.2. Controlled Formation of 3D Circular S-Doped Carbon Spheroidal Surfaces. The controlled synthesis of 3D circular S-CSN was conducted using hydrothermal treatment (HT). The HT of carbohydrates led to the formation of carbon materials based on successive condensation, polymerization, and aromatization.[43] Active doping of carbon materials with heteroatoms of S was conducted through a one-pot method with a carbon source (glucose) and a S atom source (thiourea) at an elevated temperature of 180 °C for a long time of 24 h. Thiourea acted as the S atom source and shared a similar structure with the desired carbon material. Scheme 2 shows the controlled formation of porous carbon

https://dx.doi.org/10.1021/acsabm.0c00882
ACS Appl. Bio Mater. XXXX, XXX, XXX−XXX

materials. The 3D circular shape similar to a stacked layer formation was obtained by adding the capping agent F127 as a soft template and as a directing agent. After calcination at 900 °C, F127 was removed and a porous carbon material was formed with a new spherical morphology (spheroidal structure). Various concentrations of thiourea were added to obtain two samples, namely, S-CSN-1 and S-CSN-2. For complete carbonization, the desired materials were annealed at 900 °C under N_2 flow at a rising temperature rate of 5 °C/min. The materials were placed in a desiccator until further use and labeled S-CSN-1 and S-CSN-2.

The surface morphology of the prepared materials of 3D circular S-doped carbon spheroidal surfaces was investigated using field-emission scanning electron microscopy (FE-SEM) (Figure 1). Figure 1A shows the spherical morphology of S-CSN-2 with a stacked layer of S-doped carbon-based materials. The rough surface and the small particles around the spheres form a layer-by-layer structure as the action of F127 (Figure 1Aa). The 3D orientation and shape of S-CSN with a dense nanolayer of spherule structure were formed. Figure 1Ab,Ac shows the high-magnification SEM image at various positions and cross sections in the top view (b) and side view (c) to confirm the formation of spheroidal surfaces with a curvature structure and 3D orientation. The spheres are rough with ridge ends, confirming the predicted mechanism of the formation of a spheroidal layer by layer similar to the deposition of a layer-by-layer structure along one axis. The layer size range is too small (1−2 nm) (Figure 1Ba). The presence of F127 and thiourea through carbonization leads to the formation of curvature surface with dense spherical nanolayers. Figure 1Bb,Bc shows the formation of the spheroidal stacked layer as a layer-by-layer spherical growth with open spaces between the layers. S-CSN-1 is formed by carbon layer deposition around one axis to form a spherical construct of carbon-based materials with an open holelike cavity with micropores/nanopores/macropores and grooves. The surface texture is rough with a 3D curvature structure and ridges (Figure 1Bc). Focusing on the top view of the formed spheroidal surface, a fraction of layers formed with nano-grooves inside was observed. The size of the layer ranges from 2 to 5 nm, and the full sphere size is 0.5 μm (Figure 1Bb). The atomic distribution of C, O, and S atoms on the surface of S-CSNs to determine efficient carbonization was investigated using EDX−SEM. Figure 1Ca−Cc presents the EDX−SEM map of S-CSN-2, showing the C, O, and S atomic distribution. The homogeneous distributions of C, O, and S atoms on the surface of S-CSN-2 with 63.17% C, 31.96% O, and 4.87% S are presented. The atomic contents and homogeneous distribution of C, O, and S of S-CNS-1 were observed to have different contents of C (71.36%), O (25.58%), and S (3.06%) (Figure S1Aa−Ac). The C and S contents in S-CSN-1 and S-CSN-2 vary and may influence the electrochemical activity.

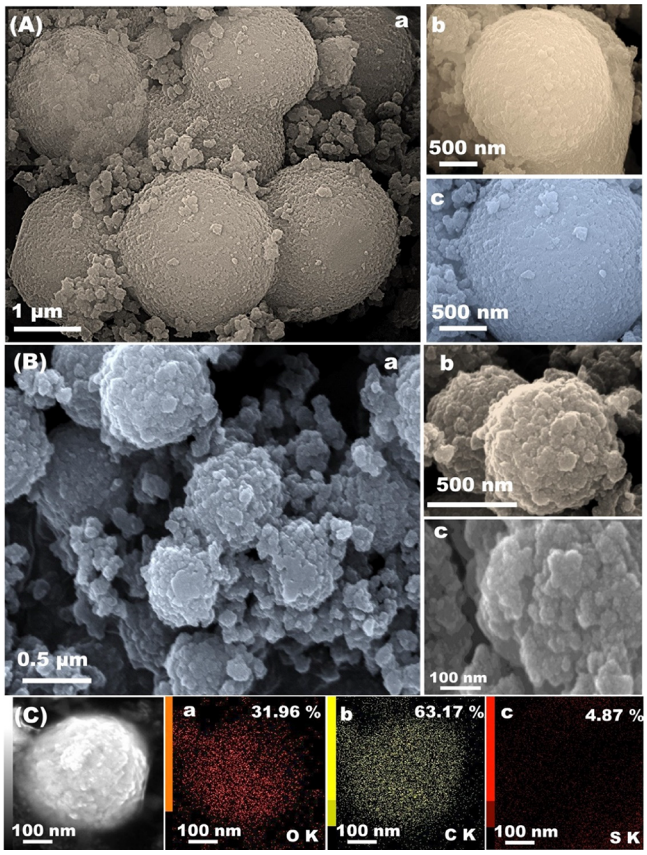

Figure 1. (A) FE-SEM-images of the S-CSN-2 with low magnification (a). (b, c) High-magnification FE-SEM-images of the outer surface topography of S-CSN-2. (B) FE-SEM-image of S-CSN-1 at low magnification (a). (b, c) High−magnification FE-SEM, focusing on the surface texture and showing the stocked layer-by-layer formation, of the 3D circular surface curvature of S-CNS-1. (C) EDX−SEM mapping of S-CSN-2 of O (a), C (b), and S (c).

Dark-field (DF) and bright-field (BF) scanning transmission electron microscopy (DF- and BF-STEM) were employed to confirm the ridge ends and curvature of the 3D spheroidal structure of S-CNS-1 (Figure 2Aa−Ac). Figure 2Aa,Ab confirms the spheroidal growth of nanolayers with an ultrathin size and the 3D orientation of S-CSN-1. BF-STEM confirms the spheroidal formation with a rough surface texture, 3D curvature orientation, and weaved surface. The dense nanolayer, ridge ends, and U-undulation are presented in Figure 2Ac. Therefore, the S-CNS surface of the heterogeneous surface of ridge ends, rough surface texture, 3D curvature orientation was successfully designed for potential sensing and biosensing application. Figure 2Ba shows the HRTEM of S-CSN-2 and reveals the spheroidal surface with a nanoporous construct and curvature surfaces. The surface ends are rough with ridge ends (Figure 2Bb). The spherical growth is similar to that observed from the deposition of a nanolayer around one axis to form spheroidal constructs and confirms the heterogeneous surface with ridge ends, a curvature, and a rough surface.

The formation of porous carbon materials and the surface area of S-CNS-1 and S-CNS-2 were evaluated using N_2 adsorption isotherms. Figure 2C shows the N_2-adsorption isotherm of S-CNS-1 (violet line) and S-CNS-2 (green line). The N_2 adsorption behavior displays a typical type I isotherm, in which a sharp uptake at low P/P_0 (P/P_0 = 0.02) and high uptake at a high relative pressure (P/P_0 > 0.9) were observed. This behavior is related to the formation of a microporous network.[44−47] Figure 2D shows the pore size distribution curves of S-CSN materials that are determined by using nonlocal density functional theory (NLDFT)-pore distribution of S-CNS-1 (violet line) and S-CNS-2 (green line), confirming the presence of microporous particles with pore sizes ranging from 1.5 to 2.2 nm. The surface areas (S_{BET}) of S-CNS-1 and S-CNS-2 are 612 and 164 m^2g^{-1}, respectively. These results illustrate the large surface area and microporous morphology of S-CNS-1. The S-CNS structure and the effect of S atoms on

https://dx.doi.org/10.1021/acsabm.0c00882
ACS Appl. Bio Mater. XXXX, XXX, XXX−XXX

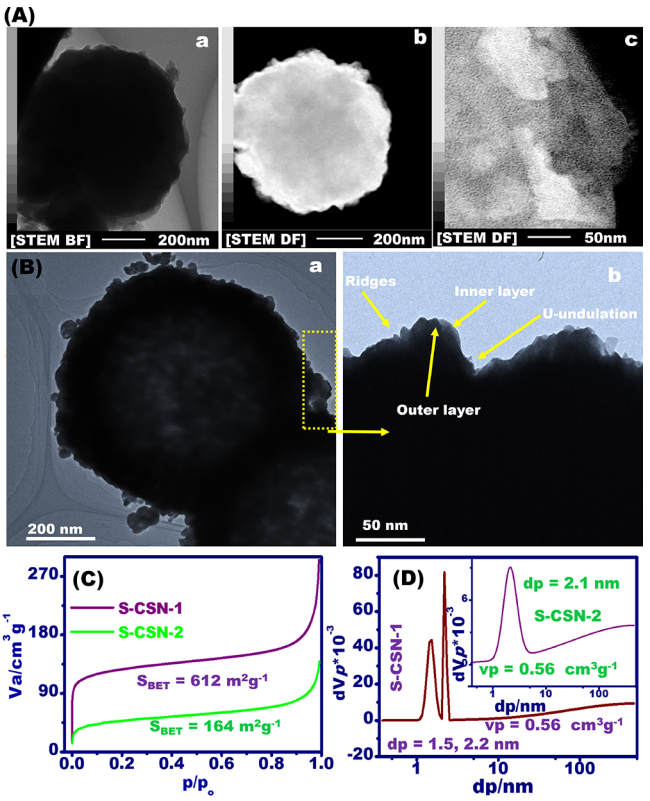

Figure 2. (A) (a) BF- and (b, c) DF-STEM images of S-CNS-1. (B) HRTEM images of S-CNS-2 with (a) focus on the spherule morphology and (b) focus on the outer surface topography. (C) N_2 adsorption isotherm of S-CSN-1 (violet line) and S-CSN-2 (green line). (D) NLDFT pore size distribution of S-CSN-1 (violet line) and S-CSN-2 (green line).

the graphitic nature were determined using Raman microscopy. Figure S1B shows two Raman shift peaks of S-CSN-1 (violet line) and S-CSN-2 (green line), centered at 1350 and 1560 cm^{-1} for the G and D bands, respectively. The presence of a G band indicates sp^2 hybridization (formation of a graphitic construction chain), while the D band indicates the distortion of the graphitic construct (sp^3 hybridization). The presence of S and O atoms in the graphitic carbon chain are indicated by the presence of the D band and indicates the distortion of the sp^2 hybridization. The I_D/I_G values of 0.89 and 0.94 for S-CSN-1 and S-CSN-2, respectively, confirm the degree of graphitization and distortion order.[48,49] These results confirm the successful doping of S atoms in the carbon-based material. In addition, the low I_D/I_G ratio for S-CNS-1 is related to the decrease in the O content, high carbon content, and the effect of the S dopant. The WA-XRD analysis has been used to investigate the carbonization process of S-CNS-1 and S-CNS-2. Figure S1C shows two broad peaks centered at 2θ = 29.65 and 42° for S-doped carbon materials in the WA-XRD spectra. These peaks are related to the formation of amorphous graphitic carbon. The presence of a peak at 2θ = 42° indicates the distortion of the graphitic construct and supports the presence of heteroatoms, such as O and S, in the graphitic chain. The XPS analysis shows three peaks at around 166, 284.28, and 527 eV for S 2p, C 1s, and O 1s, respectively, proving their presence in S-CNS (Figure S1D). The C 1s (Figure S1E), S 2p (Figure S1F), and O 1s (Figure S1G) XPS spectra show the formation of carbon materials with actively doped S atoms (for additional details, see Supporting Information). The presence of C−SO_2−C and C−SC were confirmed by XPS analysis of the S 2p spectra. Therefore, the active electrode surface of S-CNS displays strong binding and facile diffusion of NEP molecules as the presence of SO_x group at the outer surface. The designed nanosensor based on S-CNS has abundant active centers, an open and microporous network, S incorporated into the carbon chain, a rough surface texture, a 3D spheroidal orientation, and meso-grooves, forming a highly interfacial electrode surface. The electrode surface topography and thickness were investigated by AFM analysis (Scheme 1D). The AFM microscopy patterns showed that the fabricated S-CNS surface has a degree of roughness with multiple vacancies. The topographic image showing rough and heterogeneous arrangements along the electrode surfaces indicates for strong binding and facile diffusion of NEP analytics.

3.3. Catalytic Activity and Sensing Property of S-CNS.

The catalytic activity of S-CNS-1- and S-CNS-2-modified electrodes and a bare GCE was determined in $[Fe(CN)_6]^{3-}$ solution by cyclic voltammetry (CV) (Figure S2A). The S-CNS-1-modified electrode (I_a = 24.28 μA) shows the highest catalytic activity and the fastest charge transfer compared with the S-CNS-2-modified electrode (I_a = 16.02 μA) and bare GCE (I_a = 12.64 μA). This finding may be due to the effects of the topography, morphology, and chemical components of the designed electrode with a rough curvature surface, high surface area, microporous construction, and efficient S content. In addition, the active catalytic surface areas are 0.005, 0.006, and 0.009 cm^2 for the GCE and S-CNS-2- and S-CNS-1-modified electrodes, respectively, as determined by applying the Randles−Sevick formula [for more details, see Supporting Information, Figure S2A].[50] These data support the high electrode surface area and the significant increase in the sensitivity and catalytic activity of the modified electrodes.

The surface charge transfer and electron diffusion activity of the modified electrode was further confirmed. Impedance microscopy (EIS) was conducted on the S-CNS-2- and S-CNS-1-modified electrodes in 0.1 M PBS (pH =7) with 0.001 M $[Fe(CN)_6]^{3-}$ (Figure S2B).[51,52] The S-CSN-1-modified electrode shows the lowest semicircle and high diffusion line pathway compared with the S-CSN-2-modified electrode and GCE [for additional details, see Supporting Information, Figure S2B]. The S-CSN-1-modified electrode exhibits the lowest surface charge resistance and high electron diffusion. Figure S2C shows the zeta potential plot of S-CNS-1 at various pH values. The finding indicates that the overall charge onto the S-CSN-1 electrode surface is negative in the pH 6.0−8.0 range. Therefore, the negatively charged surfaces enhance the binding events with NEP molecules, leading to the high sensitivity and selectivity of the electrode. Thus, the S-CSN-1 electrode provides good electrochemical activity in terms of fast charge transport, high electron diffusion, negative surface charge, and low charge distance pathway.

The sensing property of S-CNS-1- and S-CNS-2-modified electrodes and the bare GCE for sensitive and selective signaling of NEP was determined using CV. The CV measurements illustrate the electrochemical oxidation−reduction peaks of NEP using various electrodes. As presented in Figure S2D, the oxidation−reduction peaks of 20 μM NEP were obtained for S-CNS-1- (violet line) and S-CNS-2 (green line)-modified electrodes and the GCE (black line). Various anodic and cathodic current values and applied potential peak positions were observed as the electrode changed. The S-CNS-

https://dx.doi.org/10.1021/acsabm.0c00882
ACS Appl. Bio Mater. XXXX, XXX, XXX−XXX

1-modified electrode displays higher NEP sensing property at low applied potential compared with the S-CNS-2-modified electrodes and GCE. The current values (I_a) of the anodic peaks are 33.29, 17.87, and 12.16 μA recorded at applied potentials of 0.30, 0.33, and 0.494 V for S-CNS-1, S-CNS-2, and the GCE, respectively. The S-CNS-1-modified electrode provides high sensitivity for signaling NEP at a low applied potential. These results may be related to (a) the high surface area, (b) porous construction, (c) morphology of the spherical monolayer with open spaces in between, (d) rough surface, and (e) efficient S content.[3,4,8,24] CV measurements were conducted with and without 20 μM NEP to confirm the active signaling of the S-CSN-1-modified electrode (Figure S2E). The redox peaks were observed with a high catalytic current value and may be related to the oxidation−reduction of NEP with high sensitivity. Scheme 3 illustrates the design of a sensitive NEP biosensor based on the S-CNS-modified electrode and presents the facile diffusion and binding through the porous network and activity centers. The liberated NEP form the neuronal cell line was detected. As a result of the effect of stimulating agents, the increase in the level of neurotransmitters in living cells is distinct. These results indicate that the S-CSN-1-modified electrode can be employed for sensitive signaling of NEP in various human samples for clinical applications.

Scheme 3. Visual Representation of the Biosensor and the Process of Diffusion, Binding, and Electro-oxidation of NEP in the Construct[a]

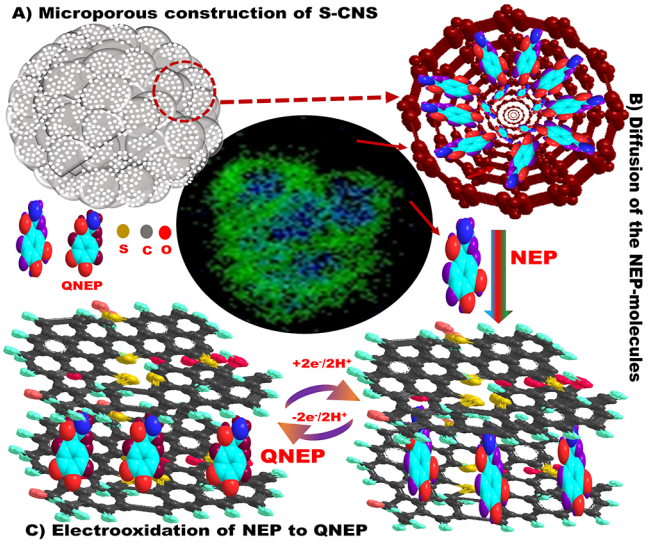

[a](A) Porous construction of S-CSN-1 with micro- and mesopore distribution. (B) Diffusion and binding of the NEP molecules through the inner/outer surface for the facile, sensitive, and selective sensor. S-CSN-1 acts as the transducing elements for highly sensitive detection of NEP. (C) At the electrode surface of S-CSN-1, the oxidation−reduction of NEP to QNEP and the reverse process with loss and acceptance of $2e^-/2H^+$ proceeded with fast charge transport and low surface resistance.

3.4. Electrochemical Set Conditions of NEP on the S-CSN-1-Modified Electrode. The CV profile was obtained at a scan rate of 100 mV/s in 0.1 M PBS with a pH range of 5−8 to study the effect of electrolyte pH on NEP oxidation−reduction. Figure 3A demonstrates the effect of electrolyte pH on the current peaks of the anode oxidation and cathode

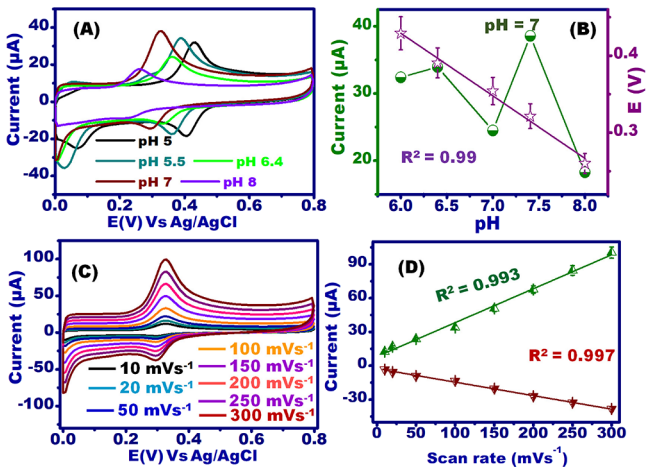

Figure 3. (A) CVs of pH-dependent monitoring assay of 20 μM NEP using the S-CSN-1-modified electrode at various pH values ranging from 5 to 8 at a scan rate of 100 mV s^{-1}, under N_2 saturation. (B) Linear and scatter plots of the pH values versus the anodic current (μA) (green scatter) and applied potential (E(V)) (violet points). (C) CVs of 20 μM NEP under various scan rates of 10−300 mV s^{-1} in 0.1 M PBS (pH = 7) on the S-CSN-1-modified electrode. (D) Plot of scan rate (mV s^{-1}) vs corresponding anodic (I_a) and cathodic (I_c) currents (μA).

reduction of the NEP target. The optimum pH−catalytic current value was found at pH = 7, which is similar to the pH of human physiological fluids. Figure 3B (green scatter) shows the scattering plot of pH versus the anodic peak current. The fluctuation in the current value indicates the significant effect of pH. The applied potential position E(V) shifted to negative values with increasing pH. The negative shift in the potential suggests the key effect of H^+ ions on the oxidation−reduction process of NEP on the S-CSN-1-modified electrode. The pH versus E(V) potential function shows a linear relationship according to the following equation of E(V) = 0.7 − 0.054pH, R^2 = 0.99 (Figure 3B [violet scattering]). The slope value is 54 mV, which is in agreement with the Nernst theoretical value of 59 mV. This finding suggests that the NEP redox mechanism follows $2e^-/2H^+$.[3,53−55]

The surface interaction property of NEP on the S-CSN-1-modified electrode was illustrated using the performance of the NEP at varying scan rates. Figure 3C shows the CV measurements of 20 μM NEP at varying scan rates of 10−300 mV s^{-1} on the S-CSN-1-modified electrode. The anodic and cathodic current values increase with increasing scan rate from 10 to 300 mV s^{-1}. By plotting the scan rate (mV s^{-1}) versus the anodic current (I_a) and cathodic current (I_c) (μA), linear relationships were obtained for both I_a and I_c, with the following equations: I_a (μA) = 8.12 + 0.3ν (mV s^{-1}), R^2 = 0.993(S/N = 3) and I_c (μA) = −2.56 − 0.119ν (mV s^{-1}), R^2 = 0.997 (S/N = 3) (Figure 3D). Thus, the overall surface interaction process is adsorption-controlled.[4,8,56,57] Moreover, the surface components of S-CNS were composed of C, S, and O atoms and formed C−S−C, C−SO_2−C, and SO_x groups along the entire inner and outer surface (see XPS, Raman, and EDX−SEM mapping analysis). The functional S-active sites and groups induce the negative charge and increase the spine density at the outer surface, as evidenced by the zeta potential plot (Figure S2C). On the other hand, the NEP acid−base behavior in reaction media leads to the formation of protonated H_3NEP^+, neutral H_2NEP, and anion $HNEP^-$

https://dx.doi.org/10.1021/acsabm.0c00882
ACS Appl. Bio Mater. XXXX, XXX, XXX−XXX

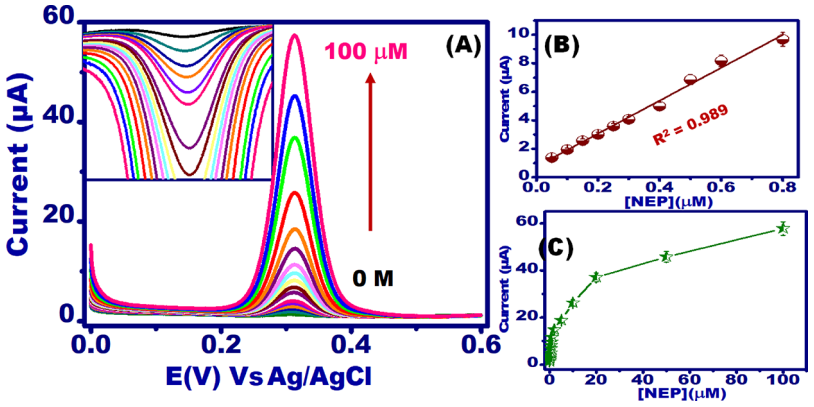

Figure 4. (A) SWV measurements of the S-CSN-1-modified electrode at various concentrations of NEP (0.01−100 μM) were performed, and the inset shows the SWV at low concentrations. (B) Calibration plot of [NEP] (μM) (0.01−0.8) versus current (μA). (C) Plot of the whole concentration range of NEP (0.01−100 μM) versus current (μA).

groups. At physiological pH (pH = 7.4) conditions, the H_3NEP^+ constituents (at pK_a = 8.64) are dominant, while the chance for the presence of the anion form is negligibly considered.[58]

This finding indicates the formation of positively charged NEP in solution. Therefore, the S-CNS−NEP interaction at the electrode surface would be strong due to the electrostatic binding between NEP molecules and functional S-active sites and groups. The current peak intensity depends on the adsorbed NEP on the S-CSN-1 electrode surface. The total adsorbed NEP amount on the S-CSN-1 electrode surface was estimated by applying the following equation[59]

$$I_p = n2F2\Gamma\nu A/4RT \quad (1)$$

where A is the bare GCE surface area, n is the number of electrons transferred, ν is the scan rate, F is the Faraday constant, T is the absolute temperature, R is the gas constant, and Γ is the total concentration of NEP on the S-CSN-1 electrode surface. The calculated Γ equals 2.82×10^{-10} mol/cm^2.

The charge transfer coefficient (α) and electron transfer rate constant (K_s) of the NEP redox reaction on the S-CSN-1-modified electrode surface can be obtained based on the relation of log ν versus the applied potential (E), within the scan rate range of 10−100 mV s^{-1}. The linear relationship of log ν versus E(V) was obtained with regression equations of E_a(V) = 0.306 + 0.009 log ν (V s^{-1}) (R^2 = 0.84) and E_c(V) = 0.326 − 0.012 log ν (V s^{-1}) (R^2 = 0.87). By applying Laviron's theory,[60]

$$\log K_a/K_c = \log \alpha/(1-\alpha) \text{or}(K_a)/K_c = \alpha/(1-\alpha) \quad (2)$$

where K_a is the slope of E_a versus log ν and equal to $2.3RT/(1-\alpha)nF$ and K_c (the slope of E_c vs log ν) is $-2.3RT/\alpha nF$. Charge transfer coefficient (α) was calculated to be 0.3 s.

The heterogeneous electron transfer rate constant (K_s) can be calculated (Laviron 1979) by applying this equation

$$\log K_s = \alpha \log(1-\alpha) + (1-\alpha)\log \alpha - \log \frac{RT}{nF\nu} - \frac{\alpha(1-\alpha)nF\Delta E_p}{2.3RT} \quad (3)$$

where α is the charge transfer coefficient, n is the number of electrons evolving from the reaction, ν is the scan rate, and ΔE_p is the anodic and cathodic peak separation potential. The K_s value is 0.25 cms^{-1}. Therefore, the S-CSN-1-modified electrode exhibits efficient and high charge transfer between the electrolyte electrode interfaces. The S-CSN nanosensor designed with specific topographical and morphological features including the 3D curvature, meso-grooves, ridge ends, rugged surface texture, S-doped the carbon chain led to the formation of a highly active surface with facile molecular/electron diffusion, multidiffusive centers, and high loading of NEP molecules.

3.5. Sensitivity, Selectivity, Stability, and Reproducibility of the S-CSN-1-Modified Electrode. The sensitive approach and the calibration curve of the S-CSN-1-modified electrode were determined using square wave voltammetry (SWV). The SWV electrochemical technique enabled the precision determination of NEP sensitivity at ultratrace concentration. Figure 4A shows the SWV measurements of various concentrations of NEP from 0.01 to 100 μM (0.1 M PBS, pH = 7) using the S-CSN-1-modified electrode. The sensitive current response was observed upon adding and increasing the concentrations of NEP. Figure 4B shows the calibration plot of NEP concentrations (μM) versus the current (μA) within the range of 0.01−0.8 μM. A linear relationship was obtained by following the equation I (μA) = 0.76 + 11.54[NEP](μM), R^2 = 0.989 (S/N = 3). The limit of detection is 0.001 μM, with a wide linear range of 0.01−0.8 μM. The linearity was distorted at high concentrations of NEP possibly due to electrode saturation (Figure 4C). These results provide a highly sensitive protocol for signaling of NEP at ultratrace levels with a wide linear range using the S-CSN-1-modified electrode. S-CSN-1 provides highly sensitive detection of NEP with low detection limits and a wide linear range and thus could be a sensitive biosensor for clinical applications. The high sensitivity with a wide linear range of S-CSN-1 may be related to the morphology of the spherical surface with a rough contact surface, an open carbon network of S dopant atoms, active functionalization of the active interfacial surface, high surface area, and microporous construction. Moreover, NEP molecules diffuse through the pores and binds strongly to the S-CSN-1 active sites, resulting in a multidiffusive electrode surface with fast charge transport.

Electrode selectivity was studied as a function of potential interfering molecules such as ascorbic acid (AA), DA, epinephrine (EP), and uric acid (UA). These biomolecules are usually present in human body fluids and overlap with the NEP oxidation peak. Figure S3 shows the column plot of NEP

https://dx.doi.org/10.1021/acsabm.0c00882
ACS Appl. Bio Mater. XXXX, XXX, XXX−XXX

concentration and the concentrations of AA, UA, DA, and EP. Meanwhile, no response of AA and UA is observed at the same detection level of NEP, and a small interfering effect is notified for DA and EP. These results provide a highly selective biosensor for signaling NEP. The designed S-CSN-1 biosensor showed the lowest detection limit compared with the other modified electrodes of various sensors (Table S1). In view of electrode applicability, the low-cost fabrication and excellent features of the portable neurotransmitter senor electrode are of interest. In this regard, the S-CNS electrode was prepared by a simple approach and a low-cost material source and exhibited sensitivity without the need for any treatment with strong acid/alkaline solutions. In addition, the S-CNS electrode has a highly stable structure (see Figure S4A). FE-SEM patterns show the structure stability of the reusable S-CNS electrode after 200 cycles, despite the electropolymerization of NEP at the electrode surface. Furthermore, the designed biosensor of S-CSN-1 showed high stability and good reproducibility, with an RSD of 1.7 up to five samples and five electrodes [for additional details, see Supporting Information, Figure S4B,C].

3.6. Selective Signaling of NEP in Human Blood Serum and Secretion from PC12 Cells under a Stimulation Agent. The validity of the biosensor for real-time monitoring of NEP in human fluids, such as human blood serum, was determined. Various amounts of NEP were spiked in 0.1 M PBS (pH = 7) containing 10 μL of human serum and measured by the SWV technique (S/N = 3). Table S2 shows the recovery of NEP on the S-CSN-modified electrode. A high recovery of the spiked samples was obtained, ranging from 98 to 99.9%. These results confirm the suitability of the S-CSN-1-modified electrode for detection of NEP in human serum samples and can be employed for clinical application due to its fast response, high sensitivity, good selectivity, and promising economic value.

Successful detection of the levels of monoamine neurotransmitters (i.e., NEP) in the samples of human tissues (neuronal cells and in the brain) is highly needed for investigation of some neurological diseases, such as schizophrenia. PC12 cells acted as the model of the nervous system cells. In vitro monitoring of NEP liberated from neuronal cells, such as PC12, was evaluated under various concentrations of stimulating agents, such as KCl solution. First, designing sensitive and selective materials with high biocompatibility opens the chance for cellular sensing applications. Thus, laser scanning confocal microscopy of S-CSN within the cells after incubation for 4 h was conducted (Figure 5A–D). S-CSN and cells were evaluated using bright-field images. S-CSN surrounded the cell membrane of PC12 (Figure 5A). Moreover, the cells were stained by phalloidin for F-actin counterstaining and the nucleus was stained by DAPI. The merged image of the cells confirmed the S-CSN biocompatibility, as presented in Figure 5B–D. The cell's cytoplasm and nucleus are not affected by S-CSN, and shrinkage of the cell membrane and change in the cell's nucleus were not observed. These data confirm the high biocompatibility of S-CSN when incubated with PC12 cells. Therefore, S-CSN exhibits potential for further in vitro and in vivo studies.

The cytotoxicity of the materials was further confirmed. The cells were grown in a 96-well plate with a concentration of 4×10^5 cells/mL. Various amounts of S-CSN (10–200 μg/mL) were incubated with the cells for 24 h by using Cell Counting Kit-8 (CCK-8) assays and measured using a microplate reader. Figure 5E shows the scatter plot of the concentrations of the

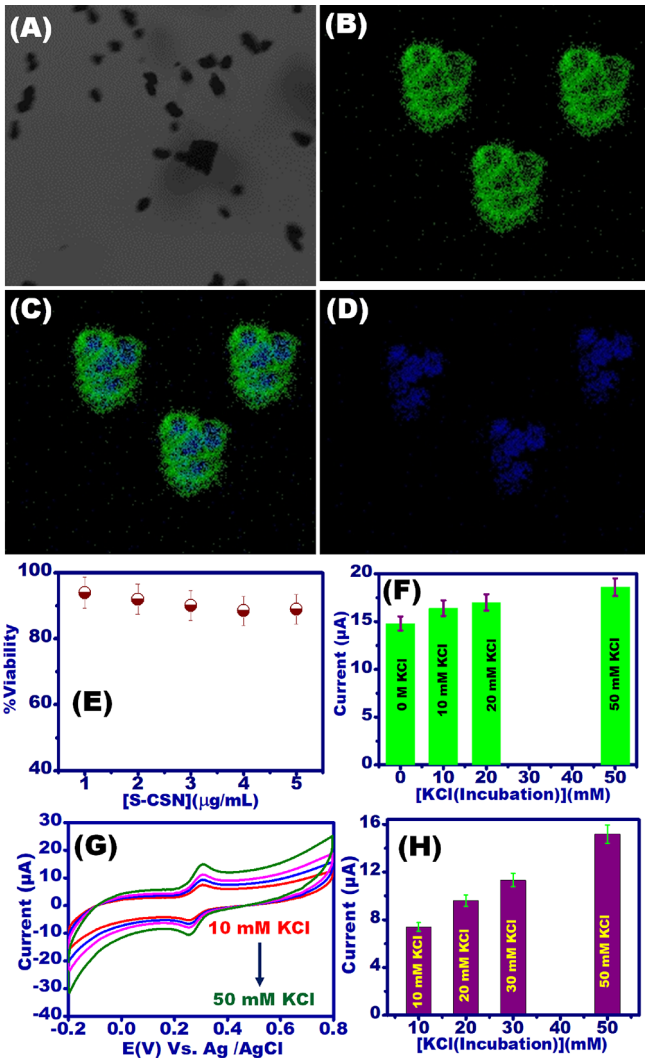

Figure 5. (A–D) Confocal microscopy images recorded at an excitation wavelength of 405 and 488 nm DAPI and phalloidin. (A) Bright-field image of S-CSN-1 incubated with PC12 cells. (B) Filamentous actin staining (phalloidin) of the PC12 cells. (C) Merged image of the nucleus and F-actin of PC12 cells upon incubation with S-CSN-1. (D) Nucleus counterstaining (DAPI) of PC12 cells. (E) Cytotoxicity assay of S-CSN-1 on the PC12 cell line with various concentrations (10–200 μg/mL) using a CCK-8 assay protocol and a microplate reader at 450 nm. (F) Column plot of the $[K^+]$ (mM) versus secreted NEP from the PC12 cells (3×10^6 cells/mL) using SWV measurements in the range of 0–50 mM. (G) CVs of cell supernatants incubated with various amounts of KCl (10–50 mM). (H) Column plot of $[K^+]$ (mM) versus secreted NEP from the PC12 cells (2×10^6 cells/mL) using CV measurements in the range of 10–50 mM.

materials versus cell viability. The plot reveals the significant low cytotoxicity of S-CSN. There was a loss of only 23% cell viability at a high concentration of 200 μg/mL and a loss of only less than 7% at 10 μg/mL. Thus, S-CSN exhibits low cytotoxicity and high biocompatibility within living cells and has high applicability for monitoring NEP in living cells.

The in vitro monitoring and setting up of the NEP biosensor protocol were performed using SWV under the optimal conditions. The NEP secreted from PC12 cells was measured by taking supernatants with 3×10^6 PC12 cells/mL and determined using the S-CSN-modified electrode. The PC12

https://dx.doi.org/10.1021/acsabm.0c00882
ACS Appl. Bio Mater. XXXX, XXX, XXX–XXX

cells were incubated with various amounts of stimulating agents (0−50 mM KCl) for 30 min. Figure 5F shows the plot of KCl concentration (mM) versus current (μA). To confirm the sensitive detection of NEP using the S-CNS-1-modified electrode, a specific concentration of NEP secreted from PC12 cells (2×10^6 cells/mL) was confirmed by CV measurements. Figure 5G shows the CVs of various cell supernatants that were incubated with various amounts of KCl (10−50 mM) for 30 min. The column plot of KCl concentrations (mM) versus the corresponding current (μA) indicates the sensitive and selective detection of NEP secreted from living cells under K^+ stimulation (Figure 5H). Extracellular NEP was stimulated in the presence of K^+ ions. The key role of K^+ ions was determined by depolarization of the cell membrane and induction of the influx of Ca^{2+} and Na^+ to open the voltage-sensitive Na^+ and Ca^{2+} channels.[4,8,61,62] The anodic current of NEP molecules secreted from the neuronal PC12 cell line model depends on K^+ concentration. Therefore, the designed biosensor of S-CSN can selectively and sensitively detect NEP in living cells. Moreover, the designed biosensor of S-CSN can be employed for clinical application and early diagnosis of some neuronal diseases, such as schizophrenia. The proposed sensing protocol exhibits high sensitivity, selectivity, low cytotoxicity, and high biocompatibility.

4. CONCLUSIONS

This work developed an NEP biosensor based on a metal-free electrode with a 3D circular surface curvature of a spherule surface (S-CSN) that has high sensitivity and selectivity, fast response, and biocompatibility. S-CSN was designed based on controlled spheroidal nanolayer formation. The 3D circular surface curvature of the spherule-based electrode was successfully fabricated from a stacked layer-by-layer approach that orientated around one axis to form ellipsoid structure morphologies. The designed electrode surface showed a 3D curvature surface, a rough surface texture with ridge ends, and bundle surface meshes. The surface topography and morphology of S-CSN exhibited the outer surface coverage of electrode sensor surfaces. The S-CSN-based biosensor possessed a highly active interfacial surface for selective detection of NEP with fast electron transfer, and facile molecular diffusion, low charge distance pathway, and strong binding to NEP molecules. S-CSN-1 provides a sensitive sensing protocol with high stability, good reproducibility, a low detection limit of 0.001 μM, and a wide linear range of 0.01−0.8 μM. The real-time monitoring of NEP in human blood serum with high recovery of (up to 99.9%) set up a readable sample based on the S-CSN-1-modified electrode. The sensing protocol could be an in vitro assay for signaling NEP from living cells. S-CSN-1 provides a highly sensitive and selective biosensor for signaling NEP in human blood samples and neuronal cells and receptors with low cytotoxicity and high biocompatibility for clinical investigation of several neuronal diseases.

■ ASSOCIATED CONTENT

Supporting Information

The Supporting Information is available free of charge at https://pubs.acs.org/doi/10.1021/acsabm.0c00882.

Materials and methods, chemical reagents, electrochemical sensing system, and characterization analysis, XPS analysis of S-CNS, catalytic activity of S-CNS-1 and S-CNS-2, and stability and reproducibility studies (PDF)

■ AUTHOR INFORMATION

Corresponding Author

Sherif A. El-Safty − *Research Center for Functional Materials, National Institute for Materials Science (NIMS), Tsukuba-shi, Ibaraki-ken 305-0047, Japan;* orcid.org/0000-0001-5992-9744; Email: sherif.elsafty@nims.go.jp

Authors

Mohammed Y. Emran − *Research Center for Functional Materials, National Institute for Materials Science (NIMS), Tsukuba-shi, Ibaraki-ken 305-0047, Japan*

Mohamed A. Shenashen − *Research Center for Functional Materials, National Institute for Materials Science (NIMS), Tsukuba-shi, Ibaraki-ken 305-0047, Japan;* orcid.org/0000-0003-1592-5877

Mahmoud M. Selim − *Department of Mathematics, Al-Aflaj College of Science and Human Studies, Prince Sattam Bin Abdulaziz University, Al-Aflaj 710-11912, Saudi Arabia*

Takashi Minowa − *Nanotechnology Innovation Station, National Institute for Materials Science (NIMS), Tsukuba 305-0047, Japan*

Ahmed Elmarakbi − *Department of Mechanical & Construction Engineering, Faculty of Engineering and Environment, Northumbria University, Newcastle upon Tyne NE1 8ST, UK*

Complete contact information is available at: https://pubs.acs.org/10.1021/acsabm.0c00882

Funding

This work was supported by the Japan Society for the Promotion of Science (JSPS), grant no. P19067.

Notes

The authors declare no competing financial interest.

■ ACKNOWLEDGMENTS

We thank Dr. Miwako Takano, Young International Research Center (ICYS), NIMS for assistance.

■ REFERENCES

(1) Casadio, S.; Lowdon, J. W.; Betlem, K.; Ueta, J. T.; Foster, C. W.; Cleij, T. J.; van Grinsven, B.; Sutcliffe, O. B.; Banks, C. E.; Peeters, M. Development of a novel flexible polymer-based biosensor platform for the thermal detection of noradrenaline in aqueous solutions. *Chem. Eng. J.* **2017**, *315*, 459−468.

(2) Moghzi, F.; Soleimannejad, J.; Sañudo, E. C.; Janczak, J. Dopamine sensing based on ultrathin fluorescent metal-organic nanosheets. *ACS Appl. Mater. Interfaces* **2020**, 44499.

(3) Emran, M. Y.; Mekawy, M.; Akhtar, N.; Shenashen, M. A.; EL-Sewify, I. M.; Faheem, A.; El-Safty, S. A. Broccoli-shaped biosensor hierarchy for electrochemical screening of noradrenaline in living cells. *Biosens. Bioelectron.* **2018**, *100*, 122−131.

(4) Emran, M. Y.; Shenashen, M. A.; Morita, H.; El-Safty, S. A. 3D-Ridge Stocked Layers of Nitrogen-Doped Mesoporous Carbon Nanosheets for Ultrasensitive Monitoring of Dopamine Released from PC12 Cells under K^+ Stimulation. *Adv. Halthcare Mater.* **2018**, 1701459.

(5) Eisenhofer, G.; Pacak, K.; Huynh, T.-T.; Qin, N.; Bratslavsky, G.; Linehan, W. M.; Mannelli, M.; Friberg, P.; Grebe, S. K.; Timmers, H. J.; Bornstein, S. R.; Lenders, J. W. M. Catecholamine metabolomic and secretory phenotypes in phaeochromocytoma. *Endocr.-Relat. Cancer* **2011**, *18*, 97.

https://dx.doi.org/10.1021/acsabm.0c00882
ACS Appl. Bio Mater. XXXX, XXX, XXX−XXX

(6) Bravo, E. L.; Tagle, R. Pheochromocytoma: state-of-the-art and future prospects. *Endocr. Rev.* **2003**, *24*, 539−553.
(7) Terbeck, S.; Savulescu, J.; Chesterman, L. P.; Cowen, P. J. Noradrenaline effects on social behaviour, intergroup relations, and moral decisions. *Neurosci. Biobehav. Rev.* **2016**, *66*, 54−60.
(8) Emran, M. Y.; Shenashen, M. A.; Morita, H.; El-Safty, S. A. One-step selective screening of bioactive molecules in living cells using sulfur-doped microporous carbon. *Biosens. Bioelectron.* **2018**, *109*, 237−245.
(9) Cova, I.; Priori, A. Diagnostic biomarkers for Parkinson's disease at a glance: where are we? *J. Neural Transm.* **2018**, *125*, 1417−1432.
(10) Cerroni, R.; Liguori, C.; Stefani, A.; Conti, M.; Garasto, E.; Pierantozzi, M.; Mercuri, N. B.; Bernardini, S.; Fucci, G.; Massoud, R. Increased Noradrenaline as an Additional Cerebrospinal Fluid Biomarker in PSP-Like Parkinsonism. *Front. Aging Neurosc.* **2020**, *12*, 126.
(11) Emran, M. Y.; Shenashen, M. A.; Mekawy, M.; Azzam, A. M.; Akhtar, N.; Gomaa, H.; Selim, M. M.; Faheem, A.; El-Safty, S. A. Ultrasensitive in-vitro monitoring of monoamine neurotransmitters from dopaminergic cells. *Sens. Actuators, B* **2018**, *259*, 114−124.
(12) Reinhoud, N. J.; Brouwer, H.-J.; van Heerwaarden, L. M.; Korte-Bouws, G. A. H. Analysis of glutamate, GABA, noradrenaline, dopamine, serotonin, and metabolites using microbore UHPLC with electrochemical detection. *ACS Chem. Neurosci.* **2013**, *4*, 888−894.
(13) Zhou, Q.; Kang, S.-Z.; Li, X.; Wang, L.; Qin, L.; Mu, J. One-pot hydrothermal preparation of wurtzite $CuGaS_2$ and its application as a photoluminescent probe for trace detection of l-noradrenaline. *Colloids Surf., A* **2015**, *465*, 124−129.
(14) Robert, F.; Bert, L.; Lambás-Señas, L.; Denoroy, L.; Renaud, B. In vivo monitoring of extracellular noradrenaline and glutamate from rat brain cortex with 2-min microdialysis sampling using capillary electrophoresis with laser-induced fluorescence detection. *J. Neurosci. Methods* **1996**, *70*, 153−162.
(15) Amiri-Aref, M.; Raoof, J. B.; Ojani, R. A highly sensitive electrochemical sensor for simultaneous voltammetric determination of noradrenaline, acetaminophen, xanthine and caffeine based on a flavonoid nanostructured modified glassy carbon electrode. *Sens. Actuators, B* **2014**, *192*, 634−641.
(16) Devnani, H.; Satsangee, S. P.; Jain, R. Nanocomposite modified electrochemical sensor for sensitive and selective determination of noradrenaline. *Mater. Today: Proc.* **2016**, *3*, 1854−1863.
(17) Akhtar, N.; Emran, M. Y.; Shenashen, M. A.; Khalifa, H.; Osaka, T.; Faheem, A.; Homma, T.; Kawarada, H.; El-Safty, S. A. Fabrication of photo-electrochemical biosensors for ultrasensitive screening of mono-bioactive molecules: the effect of geometrical structures and crystal surfaces. *J. Mater. Chem. B* **2017**, *5*, 7985−7996.
(18) Abdelwahab, A. A.; Naggar, A. H.; Abdelmotaleb, M.; Emran, M. Y. Ruthenium Nanoparticles Uniformly-designed Chemically Treated Graphene Oxide Nanosheets for Simultaneous Voltammetric Determination of Dopamine and Acetaminophen. *Electroanalysis* **2020**, 2156.
(19) Taei, M.; Jamshidi, M. S. A voltammetric sensor for simultaneous determination of ascorbic acid, noradrenaline, acetaminophen and tryptophan. *Microchem. J.* **2017**, *130*, 108−115.
(20) Beitollahi, H.; Mohammadi, S. Selective voltammetric determination of norepinephrine in the presence of acetaminophen and tryptophan on the surface of a modified carbon nanotube paste electrode. *Mater. Sci. Eng. C* **2013**, *33*, 3214−3219.
(21) Pahlavan, A.; Gupta, V. K.; Sanati, A. L.; Karimi, F.; Yoosefian, M.; Ghadami, M. ZnO/CNTs nanocomposite/ionic liquid carbon paste electrode for determination of noradrenaline in human samples. *Electrochim. Acta* **2014**, *123*, 456−462.
(22) Siuzdak, K.; Ficek, M.; Sobaszek, M.; Ryl, J.; Gnyba, M.; Niedziałkowski, P.; Malinowska, N.; Karczewski, J.; Bogdanowicz, R. Boron-enhanced growth of micron-scale carbon-based nanowalls: a route toward high rates of electrochemical biosensing. *ACS Appl. Mater. Interfaces* **2017**, *9*, 12982−12992.
(23) Cha, C.; Shin, S. R.; Annabi, N.; Dokmeci, M. R.; Khademhosseini, A. Carbon-based nanomaterials: multifunctional materials for biomedical engineering. *ACS Nano* **2013**, *7*, 2891−2897.
(24) Emran, M. Y.; Shenashen, M. A.; Abdelwahab, A. A.; Abdelmottaleb, M.; El-Safty, S. A. Facile synthesis of microporous sulfur-doped carbon spheres as electrodes for ultrasensitive detection of ascorbic acid in food and pharmaceutical products. *New J. Chem.* **2018**, *42*, 5037−5044.
(25) Lu, C.; Liu, Y.; Ying, Y.; Liu, J. Comparison of MoS_2, WS_2, and graphene oxide for DNA adsorption and sensing. *Langmuir* **2017**, *33*, 630−637.
(26) Raphey, V. R.; Henna, T. K.; Nivitha, K. P.; Mufeedha, P.; Sabu, C.; Pramod, K. Advanced biomedical applications of carbon nanotube. *Mater. Sci. Eng. C* **2019**, *100*, 616−630.
(27) Alim, S.; Vejayan, J.; Yusoff, M. M.; Kafi, A. K. M. Recent uses of carbon nanotubes & gold nanoparticles in electrochemistry with application in biosensing: A review. *Biosens. Bioelectron.* **2018**, *121*, 125−136.
(28) Shenashen, M. A.; Hassen, D.; El-Safty, S. A.; Isago, H.; Elmarakbi, A.; Yamaguchi, H. Axially oriented tubercle vein and X-crossed sheet of N-Co_3O_4@ C hierarchical mesoarchitectures as potential heterogeneous catalysts for methanol oxidation reaction. *Chem. Eng. J.* **2017**, *313*, 83−98.
(29) Ding, X.; Bai, J.; Xu, T.; Li, C.; Zhang, H.-M.; Qu, L. A novel nitrogen-doped graphene fiber microelectrode with ultrahigh sensitivity for the detection of dopamine. *Electrochem. Commun.* **2016**, *72*, 122−125.
(30) Fan, S.; Zhao, M.; Ding, L.; Liang, J.; Chen, J.; Li, Y.; Chen, S. Synthesis of 3D hierarchical porous Co_3O_4 film by eggshell membrane for non-enzymatic glucose detection. *J. Electroanal. Chem.* **2016**, *775*, 52−57.
(31) Khalifa, H.; El-Safty, S. A.; Reda, A.; Shenashen, M. A.; Selim, M. M.; Elmarakbi, A.; Metawa, H. A. Theoretical and Experimental Sets of Choice Anode/Cathode Architectonics for High-Performance Full-Scale LIB Built-up Models. *Nano-Micro Lett.* **2019**, *11*, 84.
(32) Khalifa, H.; El-Safty, S. A.; Reda, A.; Shenashen, M. A.; Elmarakbi, A.; Metawa, H. A. Structurally Folded Curvature Surface Models of Geodes/Agate Rosettes (Cathode/Anode) as Vehicle/Truck Storage for High Energy Density Lithium-Ion Batteries. *Batteries Supercaps* **2020**, *3*, 76−92.
(33) Khalifa, H.; Shenashen, M. A.; Reda, A.; Selim, M. M.; Elmarakb, A.; El-Safty, S. A. Complex Structure Model Mutated Anode/Cathode Electrodes for Improving Large-Scale Battery Designs. *ACS Appl. Energy Mater.* **2020**, *3*, 9168−9181.
(34) Gomaa, H.; Khalifa, H.; Selim, M. M.; Shenashen, M. A.; Kawada, S.; Alamoudi, A. S.; Azzam, A. M.; Alhamid, A. A.; El-Safty, S. A. Selective, photoenhanced trapping/detrapping of arsenate anions using mesoporous blobfish head TiO2 monoliths. *ACS Sustainable Chem. Eng.* **2017**, *5*, 10826−10839.
(35) Gomaa, H.; Shenashen, M. A.; Yamaguchi, H.; Alamoudi, A. S.; El-Safty, S. A. Extraction and recovery of Co^{2+} ions from spent lithium-ion batteries using hierarchical mesosponge γ-Al_2O_3 monolith extractors. *Green Chem.* **2018**, *20*, 1841−1857.
(36) Shenashen, M. A.; Hassen, D.; El-Safty, S. A.; Selim, M. M.; Akhtar, N.; Chatterjee, A.; Elmarakbi, A. Mesoscopic Fabric Sheet Racks and Blocks as Catalysts with Efficiently Exposed Surfaces for Methanol and Ethanol Electrooxidation. *Adv. Mater. Interfaces* **2016**, *3*, 1600743.
(37) Li, J.; Jiang, J.; Feng, H.; Xu, Z.; Tang, S.; Deng, P.; Qian, D. Facile synthesis of 3D porous nitrogen-doped graphene as an efficient electrocatalyst for adenine sensing. *RSC Adv.* **2016**, *6*, 31565−31573.
(38) Li, R.; Wei, Z.; Gou, X.; Xu, W. Phosphorus-doped graphene nanosheets as efficient metal-free oxygen reduction electrocatalysts. *RSC Adv.* **2013**, *3*, 9978−9984.
(39) Sheng, Q.; Liu, R.; Zheng, J. Fullerene−nitrogen doped carbon nanotubes for the direct electrochemistry of hemoglobin and its application in biosensing. *Bioelectrochemistry* **2013**, *94*, 39−46.

https://dx.doi.org/10.1021/acsabm.0c00882
ACS Appl. Bio Mater. XXXX, XXX, XXX−XXX

(40) Sheng, Z.-H.; Gao, H.-L.; Bao, W.-J.; Wang, F.-B.; Xia, X.-H. Synthesis of boron doped graphene for oxygen reduction reaction in fuel cells. *J. Mater. Chem.* **2012**, *22*, 390−395.
(41) Jeon, I.-Y.; Zhang, S.; Zhang, L.; Choi, H.-J.; Seo, J.-M.; Xia, Z.; Dai, L.; Baek, J.-B. Edge-selectively sulfurized graphene nanoplatelets as efficient metal-free electrocatalysts for oxygen reduction reaction: the electron spin effect. *Adv. Mater.* **2013**, *25*, 6138−6145.
(42) Huang, B.; Hu, X.; Liu, Y.; Qi, W.; Xie, Z. Biomolecule-derived N/S co-doped CNT-graphene hybrids exhibiting excellent electrochemical activities. *J. Power Sources* **2019**, *413*, 408−417.
(43) Wang, Q.; Li, H.; Chen, L.; Huang, X. Novel spherical microporous carbon as anode material for Li-ion batteries. *Solid State Ionics* **2002**, *152-153*, 43−50.
(44) El-Safty, S. A.; Shenashen, M. A.; Ismael, M.; Khairy, M. Mesocylindrical Aluminosilica Monolith Biocaptors for Size-Selective Macromolecule Cargos. *Adv. Funct. Mater.* **2012**, *22*, 3013−3021.
(45) El-Safty, S. A.; Sakai, M.; Selim, M. M.; Hendi, A. A. Mesosponge optical sinks for multifunctional mercury ion assessment and recovery from water sources. *ACS Appl. Mater. Interfaces* **2015**, *7*, 13217−13231.
(46) Elshehy, E. A.; EL-Safty, S. A.; Shenashen, M. A. Reproducible design for the optical screening and sensing of Hg (II) ions. *Chemosensors* **2014**, *2*, 219−234.
(47) Khairy, M.; El-Safty, S. A. Promising supercapacitor electrodes based immobilization of proteins onto macroporous Ni foam materials. *J. Energy Chem.* **2015**, *24*, 31−38.
(48) Sun, Y.; Wu, J.; Tian, J.; Jin, C.; Yang, R. Sulfur-doped carbon spheres as efficient metal-free electrocatalysts for oxygen reduction reaction. *Electrochim. Acta* **2015**, *178*, 806−812.
(49) Kim, H.-T.; Shin, H.; Jeon, I.-Y.; Yousaf, M.; Baik, J.; Cheong, H.-W.; Park, N.; Baek, J.-B.; Kwon, T.-H. Carbon−Heteroatom Bond Formation by an Ultrasonic Chemical Reaction for Energy Storage Systems. *Adv. Mater.* **2017**, *29*, 1702747.
(50) Buttry, D. *Electroanalytical chemistry*; Bard, A., Ed., Vol. *17*. Marcel Dekker: New York, 1991.
(51) Akhtar, N.; El-Safty, S. A.; Abdelsalam, M. E.; Kawarada, H. One-pot fabrication of dendritic NiO@ carbon−nitrogen dot electrodes for screening blood glucose level in diabetes. *Adv. Healthcare Mater.* **2015**, *4*, 2110−2119.
(52) Akhtar, N.; El-Safty, S. A.; Abdelsalam, M. E.; Shenashen, M. A.; Kawarada, H. Radially oriented nanostrand electrodes to boost glucose sensing in mammalian blood. *Biosens. Bioelectron.* **2016**, *77*, 656−665.
(53) Emran, M. Y.; El-Safty, S. A.; Shenashen, M. A.; Minowa, T. A well-thought-out sensory protocol for screening of oxygen reactive species released from cancer cells. *Sens. Actuators, B* **2019**, *284*, 456−467.
(54) Emran, M. Y.; Khalifa, H.; Gomaa, H.; Shenashen, M. A.; Akhtar, N.; Mekawy, M.; Faheem, A.; El-Safty, S. A. Hierarchical CN doped NiO with dual-head echinop flowers for ultrasensitive monitoring of epinephrine in human blood serum. *Microchim. Acta* **2017**, *184*, 4553−4562.
(55) Li, Y.; Gu, Y.; Zheng, B.; Luo, L.; Li, C.; Yan, X.; Zhang, T.; Lu, N.; Zhang, Z. A novel electrochemical biomimetic sensor based on poly (Cu-AMT) with reduced graphene oxide for ultrasensitive detection of dopamine. *Talanta* **2017**, *162*, 80−89.
(56) Emran, M. Y.; Shenashen, M. A.; Abdelwahab, A. A.; Abdelmottaleb, M.; Khairy, M.; El-Safty, S. A. Nanohexagonal Fe_2O_3 electrode for one-step selective monitoring of dopamine and uric acid in biological samples. *Electrocatalysis* **2018**, *9*, 514−525.
(57) Emran, M. Y.; Shenashen, M. A.; Abdelwahab, A. A.; Khalifa, H.; Mekawy, M.; Akhtar, N.; Abdelmottaleb, M.; El-Safty, S. A. Design of hierarchical electrocatalytic mediator for one step, selective screening of biomolecules in biological fluid samples. *J. Appl. Electrochem.* **2018**, *48*, 529−542.
(58) Álvarez-Diduk, R.; Galano, A. Adrenaline and noradrenaline: protectors against oxidative stress or molecular targets? *J. Phys. Chem. B* **2015**, *119*, 3479−3491.
(59) Bard, A. J.; Faulkner, L. R. *Electrochemical methods and applications*; Wiley-Interscience: New York; London, 2000, *No.45314787*.
(60) Laviron, E. General expression of the linear potential sweep voltammogram in the case of diffusionless electrochemical systems. *J. Electroanal. Chem. Interfacial Electrochem.* **1979**, *101*, 19−28.
(61) Shinohara, H.; Sakai, Y.; Mir, T. A. Real-time monitoring of intracellular signal transduction in PC12 cells by two-dimensional surface plasmon resonance imager. *Anal. Biochem.* **2013**, *441*, 185−189.
(62) Mir, T. A.; Akhtar, M. H.; Gurudatt, N. G.; Kim, J.-I.; Choi, C. S.; Shim, Y.-B. An amperometric nanobiosensor for the selective detection of K^+-induced dopamine released from living cells. *Biosen. Bioelectron.* **2015**, *68*, 421−428.

https://dx.doi.org/10.1021/acsabm.0c00882
ACS Appl. Bio Mater. XXXX, XXX, XXX−XXX